Sensitivity modelling with objective damage assessment of unreinforced masonry façades undergoing different subsidence settlement patterns

Prosperi, Alfonso; Longo, Michele; Korswagen, Paul A.; Korff, Mandy; Rots, Jan G.

DOI
10.1016/j.engstruct.2023.116113

Publication date
2023

Document Version
Final published version

Published in
Engineering Structures

Citation (APA)
Prosperi, A., Longo, M., Korswagen, P. A., Korff, M., & Rots, J. G. (2023). Sensitivity modelling with objective damage assessment of unreinforced masonry façades undergoing different subsidence settlement patterns. *Engineering Structures*, *286*, Article 116113. https://doi.org/10.1016/j.engstruct.2023.116113

Engineering Structures 286 (2023) 116113

Contents lists available at ScienceDirect

Engineering Structures

journal homepage: www.elsevier.com/locate/engstruct

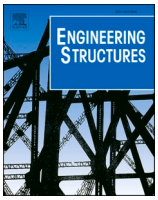

Sensitivity modelling with objective damage assessment of unreinforced masonry façades undergoing different subsidence settlement patterns

Alfonso Prosperi [a,*], Michele Longo [a], Paul A. Korswagen [a], Mandy Korff [a,b], Jan G. Rots [a]

[a] Delft University of Technology, Faculty of Civil Engineering and Geosciences, Stevinweg 1, 2628 CN Delft, 2600 GA Delft, the Netherlands
[b] Deltares, P.O BOX, 177, 2600 MH Delft, the Netherlands

ARTICLE INFO

Keywords:
Numerical modelling
Unreinforced masonry
Settlement
Cracking
Damage assessment

ABSTRACT

This study aims to investigate the damage response of unreinforced masonry (URM) façades resting on strip foundations and subjected to ground settlements via numerical models. The models depict the non-linear constitutive behaviour of both the masonry, via smeared cracking, and of the soil-foundation interaction, via nonlinear interface elements. The influence of building features, such as the masonry material, the length over height (L/H) ratio of the geometry, the wall thickness, the number and size of openings and different types of strip foundations (i.e. reinforced concrete and unreinforced) is examined. A sensitivity study additionally investigates the influence of the interface stiffness and its constitutive model. A Gaussian curve is used to replicate the shape of the ground settlements; These simulate the loss of support underneath the foundation due to urban subsidence. Eight settlement shapes are applied in the FE models, including both symmetric and asymmetric profiles, while the angular distortion is used to measure their intensity. A new aspect is that the extent of the induced damage to the façade is assessed objectively using a damage parameter that represents the number, length and width of cracks in a single scalar value. The method distinguishes between the applied settlement profile at the bottom of the interface and the retrieved settlement profile measured on the façade. The analyses indicate that for a value of the angular distortion equal to 2 ‰ (or 1/500), computed from the resulting deformations of the façades, 60% of the models exhibit serviceability damage associated with cracks of about 5 mm width. Accordingly, the limit values available in the literature are observed to be too optimistic and not conservative in relation to the analyses presented in this study. A key outcome is that facades with an L/H smaller or equal to 1 do not exhibit cracks wider than 1 mm. Façades on reinforced concrete foundations were observed to be less susceptible to settlement damage, compared to unreinforced ones.

1. Introduction

In the Netherlands, many low-rise (e.g. terraced and detached houses) unreinforced masonry (URM) buildings suffer from deformations due to subsidence phenomena. Different damage parameters are typically used to define the intensity of the subsidence-related settlements and define their relationship with the induced damage to buildings [1–5]. Examples of such proxy parameters, namely settlement-related intensity parameters (SRI) [1,2,6], are the differential settlement, rotation, angular distortion (or relative rotation), deflection ratio, or the induced strains in the building [2]. For all SRIs parameters, it is common to assume that exceeding a limit value corresponds to reaching a particular damage state. However, several uncertainties are involved when using limit values, such as: i) the limit values are random variables, strongly depending on the type of building and its features; ii) The information about the building's features as well as monitoring measurements are usually not available for a large number of buildings; iii) the induced damage depends not only on the magnitude, but also on the rate and the shape of the settlement displacements over the length of the building. Moreover, challenges arise in the classification of the damage severity exhibited by the buildings employing the available damage scales; These are based on the maximum recorded crack width and brief descriptions of the damage, while other parameters should be considered, such as the cracks' length and their number [7,8].

This study aims to evaluate the response of URM façades on strip foundations subjected to ground settlements using non-linear finite element FE models. As a novelty, the damage to the structure is computed from the results of the FE models by means of a scalar

* Corresponding author.
E-mail address: a.prosperi@tudelft.nl (A. Prosperi).

https://doi.org/10.1016/j.engstruct.2023.116113
Received 8 September 2022; Received in revised form 20 January 2023; Accepted 4 April 2023
Available online 17 April 2023

parameter; This provides an objective assessment of the damage level based on the cracks' number, width and length. A distinction is made between the applied settlements, representing the loss of support underneath the foundation, and the retrieved displacements measured at the façade. This allows studying the influence of the building's features and shape of the settlements on the relationship between the applied settlements, the façade deformation and the resulting damage.

The paper begins with a detailed description of the methodology, the FE models and the investigated variations in section 2. The outcomes of the simulations are presented in section 3 (results). In section 4 the findings of this study are discussed, and the main conclusions are presented in section 5.

2. Methodology

The analysis procedure followed consists of two main steps (Fig. 1). In Step 1 (Fig. 1), masonry façades were modelled in 2D plane stress with the software Diana FEA 10.5, including different materials, geometries, soil conditions and settlement loads.

All the investigated parameters are schematically presented in Fig. 2. Particularly, below the façade, the strip foundation systems were explicitly modelled, to further investigate their role. Moreover, class-III Mindlin beam elements were placed on the two lateral sides of the façades to simulate the presence of transversal walls and transverse foundations; This was observed to aid the development of realistic crack patterns due to ground settlements [9]. The lateral beam elements simulate the additional stiffness at the sides of the façade due to the interlocking with the house-to-house separation walls which restrain the rotation of the façade's edges [9]. The models include openings underneath masonry lintels and 8-node quadratic plane stress elements with 3 × 3 Gaussian integration schemes were adopted for the façade, lintels and strip foundation, with a mesh size of 100 mm × 100 mm. Three-noded elements were used for the beam elements, while six-noded line interface elements with the Lobatto integration scheme [10] were used to model the soil-foundation interaction, both with a mesh size of 100 mm. The geometry (i.e. length L, height H, opening percentage in Fig. 2), the material properties (i.e. the elastic-softening orthotropic material properties), the strip foundation system and the type of soil were varied to investigate their effect on the structural response in terms of damage. Eight settlement configurations were considered to simulate the symmetric and non-symmetric hogging and sagging profiles due to the loss of support underneath the foundation. The settlement profiles specifically aim to represent urban subsidence phenomena and differ from those by excavations, tunnelling or mining works [11–13].

In Step 2 (Fig. 1), the output of the numerical analyses was used to retrieve the relationship between the settlement profiles and the damage. The vertical displacements at the façade's base (top edge of the foundation) of all the models were selected to output the façade's displacements. In this regard, this study is framed distinguishing with the term "applied" the prescribed displacements at the bottom of the interface (Fig. 2), while the term "retrieved" is used for the resulting displacements at the façade's base (i.e. top edge of the strip foundation). The crack widths at the integration points of the façade are used to quantify the extension and accumulation of the damage. The relationships between the applied, retrieved displacements (in terms of differential settlement, rotation, angular distortion and deflection ratio [2]) and the damage severity were then determined.

2.1. Façade and foundation variations

A two-storey façade model with a total height of 7 m and a length of 8 m was selected as the reference case (Fig. 3f). Additional geometries were modelled varying the length over height (L/H) ratio ranging from 0.57 in Fig. 3a1 up to 5.00 in Fig. 3e2. The dimensions of the openings for the reference façade were set to ensure similarity to previous studies (e.g. Giardina et al., 2013 [14]) and corresponds to an opening percentage of 0.27. Additionally, two extra opening percentages of 0.10 and 0.20 were obtained by arbitrarily modifying the height of the openings, as shown in Fig. 3h and g respectively, for the purpose of the sensitivity analyses. The load and the effect of the floors and roof are not included in the models; Thus, in terms of mass loads the façades are only loaded by their self-weight. A wall thickness of 210 mm was considered for all analyses ("t" in Fig. 2). Such wall thickness was applied also to the lateral beam elements. A model was developed in which the lateral beam elements were not included, to further investigate their influence.

Each façade model rests on a URM strip foundation (Fig. 4a). Additional reinforced concrete (RC) strip foundations were also modelled. Among those, a RC block foundation (Fig. 4b), a RC strip foundation with a masonry layer on top (Fig. 4c) and a RC strip foundation with a RC stiffening beam (Fig. 4d). The top edge of each foundation system corresponds to the ground surface level. The longitudinal (i.e. along the façade) rebar system was modelled as line reinforcement and considered fully embedded in the concrete and no slipping behaviour was considered. The equivalent cross-section of the steel is shown in Fig. 4 for each RC foundation.

2.2. Material properties

The parameters of five different sets of masonry materials were retrieved from the Dutch Standard [15] and previous studies [16,17] to investigate the response of both: baked clay (BC) and calcium-silicate (CS) brick masonry. Accordingly, in Table 1, the material properties are reported as: i) M2 represents the material properties of a BC brickwork, built before 1945, ii) M1 a poor version of M2 where the elastic and strength parameters were reduced by 50% to simulate the effect of an aged pre-damaged material, as advised in the Standard [15], iii) M3 is the material set used for clay masonry built after 1945, iv) M4 represents a CS brickwork with general purpose mortar and v) M5 a CS block or large element masonry with thin mortar layers. The masonry façades are supposed to be built with a running bond pattern, with typical brick dimensions of 210x50x100 mm for the BC bricks and 210x70x100 mm for the CS bricks. The mortar thickness is assumed to be 10 mm. An orthotropic, smeared crack/shear/crush constitutive law was employed to explicitly simulate the cracking behaviour of masonry.

This constitutive model labelled as EMM (Engineering Masonry Model, [16]) is total-strain based and it describes tensile cracking, shear slip and compression crushing including their softening and specific unloading/reloading behaviour in the pre-fixed x,y-system aligned with

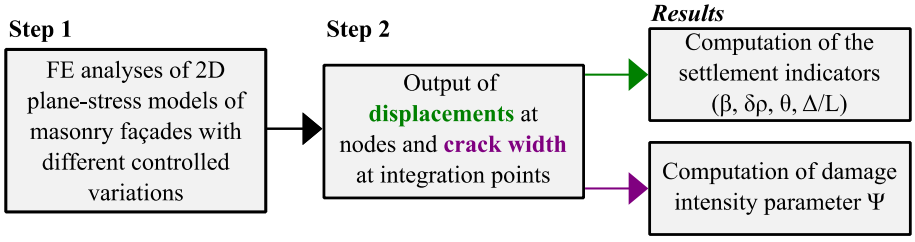

Fig. 1. Flowchart of the adopted procedure.

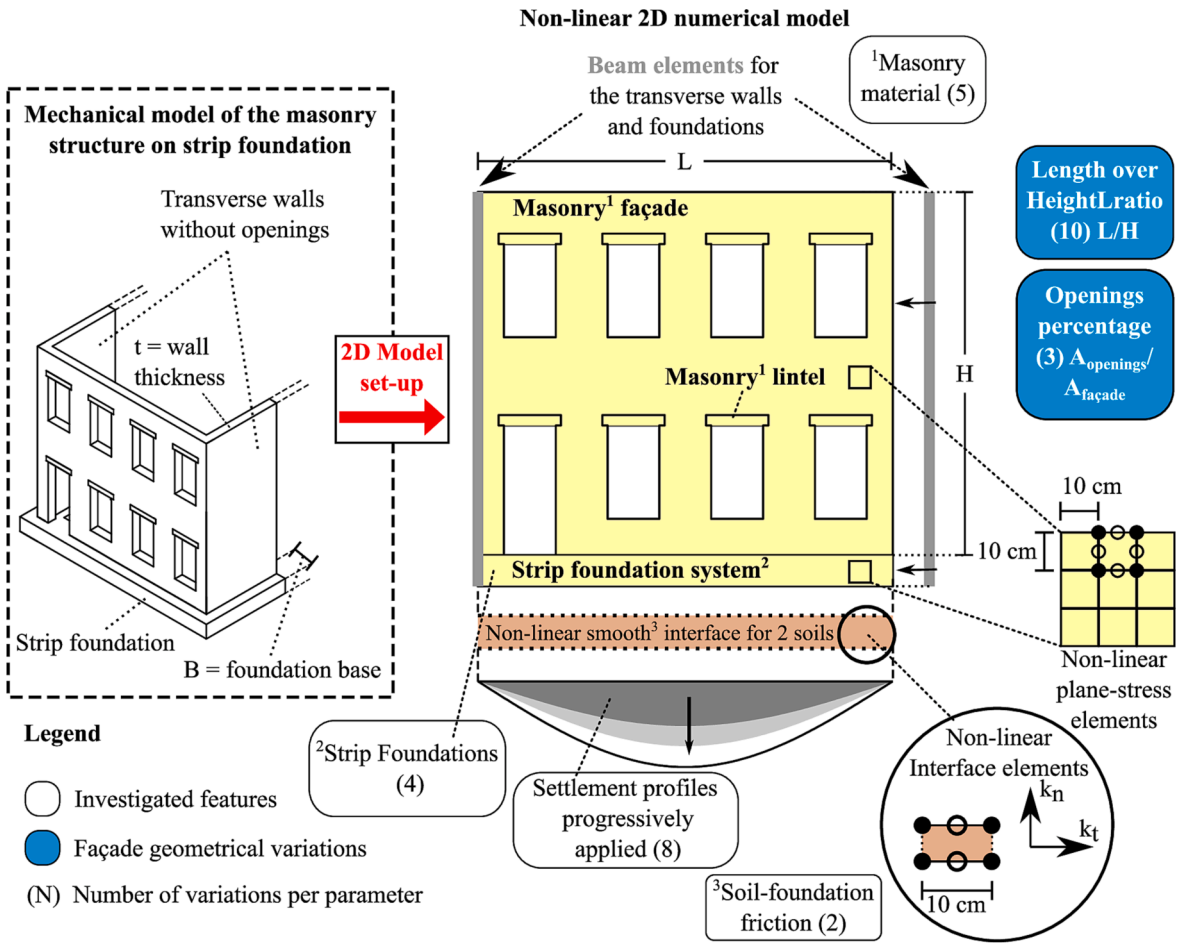

Fig. 2. Illustration of the intended mechanical model and the adopted FE modelling approach, the features included and the variations investigated. Number of variations per parameter indicated in parenthesis (N). The foundation systems adopted in the model are shown in detail in Fig. 4, while the settlement profiles applied at the bottom edge of the interface are shown in Fig. 5.

the masonry bed and head joint orientations [18]. The selected material properties were applied to both façade and masonry foundation. For the lintels the same material properties were employed (Table 1), and a rotation of 90° of the local axes was applied to account for the different orientation of the masonry (soldier brick pattern). The head-joint failure (representing vertical cracking) is based on friction, so that a higher vertical pre-compression positively contributes to the crack formation. The minimum head-joint strength (as no pre-compression is present) is set to 1.5 times the bed-joint tensile strength. The lateral beam elements make use of a linear elastic model, with the Young's modulus equal to 1/3 of the E_y for each M material, the Poisson's ratio of 0.15 and the same mass density of the considered M material [9]. The long-term effects such as creep and relaxation of the masonry material were not included, due to a lack of available information. Moreover, there may be a discrepancy between the material properties of real full scale masonry walls and those of the small-scale masonry laboratory test specimens on which the material properties of this study were based, even if these originate from real buildings.

For the variations with reinforced concrete foundations (Fig. 4b, c and d), the non-linearity of the material was explicitly modelled with the Total Strain Rotating Crack Model. The Von Mises Plasticity model was employed for the steel material of the rebar in the RC foundations. A summary of such material properties is shown in Table 2.

2.3. Applied settlement configurations

In this paper, eight possible settlement profiles were considered, reflecting symmetric and non-symmetric hogging and sagging shapes; Moreover, the settlement shapes reflect different positions of the building on a long Gaussian settlement trough [19], described by equation (1), as sketched in Fig. 5.

$$S_{v(x)} = S_{v,max} e^{\left(\frac{-x^2}{2x_i^2}\right)} \quad (1)$$

Where x is the horizontal distance from the symmetry axis of the curve and x_i is the distance from the symmetry axis of the curve to the point of inflection. Although Gaussian curves are typically adopted for tunnelling-induced, mining-induced or excavation-induced ground movements, they are herein employed to simulate the loss of support underneath the foundation due to urban subsidence processes (e.g. organic soil oxidation, soil shrinkage, groundwater lowering, etc.).

The angular distortion β was chosen to characterize the intensity of the profiles and to allow for comparison to previous studies [20–23]. It is worth stressing that the angular distortion refers to the slope of the line joining two consecutive points in relation to a line joining the two points at the sides of the façade [2]. Therefore, depending on the shape, a maximum vertical settlement $S_{v,max}$ was imposed to ensure an identical distortion, equal to 1/10, in all the profiles. In other words, the maximum settlement of each of the considered shapes differs, while the angular distortion is the same (Fig. 5).

The FE analyses make use of a two-steps procedure: first, the gravity load (referred as "Gravity" in Table 3) was applied to the structure to compute the stress states due to the self-weight; the displacement field of the façade, characterized by displacements in the order of tenths of a

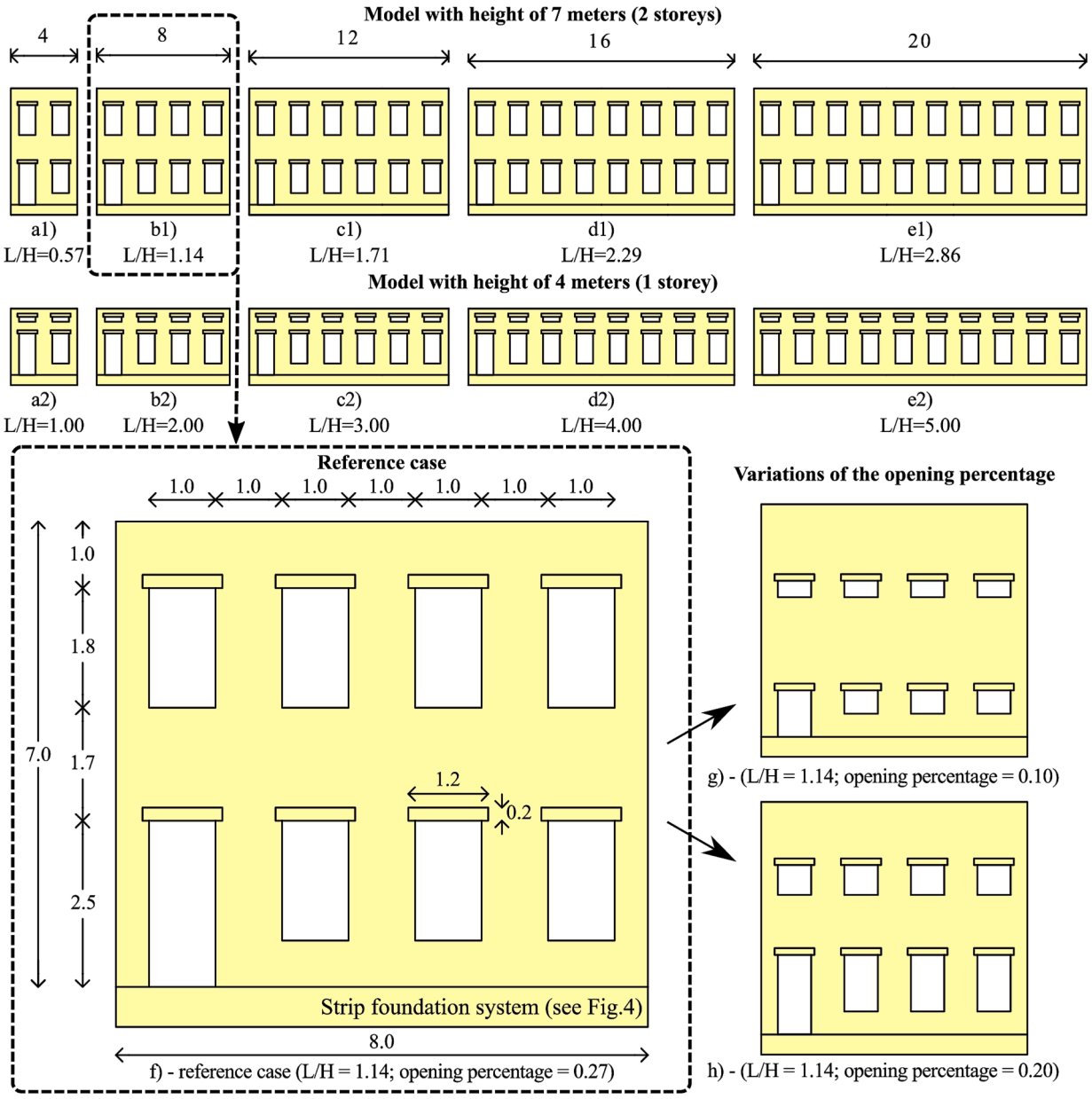

Fig. 3. Reference geometries for the masonry façade. The geometries from a1) to e2) are characterized by an opening ratio ($A_{opening}/Af_{açade}$) of 0.27. The model f) represents the reference case. The height of the openings of f) is modified arbitrarily for the geometries g) and h) to obtain the two selected opening percentages (i.e. 0.10 and 0.20 respectively). The foundation systems adopted in the model are shown in detail in Fig. 4. Not to scale. Measures in meters.

millimetre, was then cleared to avoid the occurrence of deformations not related to the applied settlements. Then, the settlement profiles (referred as "Settlement" in Table 3) were applied as prescribed nodal displacements at the bottom of the interface elements that simulate the soil-foundation interaction. The gravity load was applied in 10 steps. The number of steps used for the application of the settlements differs per shape. Three intervals with different step sizes were considered, in order to better observe the progression of the damage in the numerical model: i) 0.1 mm/step for a vertical displacement minor or equal to 10 mm, then ii) 0.2 mm/step for a vertical displacement minor or equal to 100 mm and finally iii) 0.5 mm/step for higher vertical displacements. In this way, the angular distortion was progressively increased from 0 (in the first step after the application of the gravity load) up to the 1/10. The variable step sizes ensure convergence after the occurrence of cracking and nonlinearity. Both the gravity and the settlement loads make use of the Quasi-Newton incremental-iterative procedure (also referred as "Secant method" [10]). Additional information about the iterative procedure is reported in Table 3.

2.4. Interface properties representing the soil-foundation interface

The interface between soil and foundation was modelled by selecting a no-tension smooth discrete cracking model as constitutive law for the interface elements. Such an interface is added to avoid the application of the imposed settlement directly to the strip foundation. This means that no forces (either normal or tangential) were transferred at the interface level when normal tensile stresses were acting at the base of the model. With this approach, the applied settlement displacements do not pull the façade downward, as its self-weight makes the façade deform due to the loss of support. The interface normal and tangential stiffnesses were computed using the equations reported by NEHRP [24] and proposed by Gazetas [25] and Mylonakis et al. [26], for arbitrarily shaped foundations on a homogeneous half-space [27]:

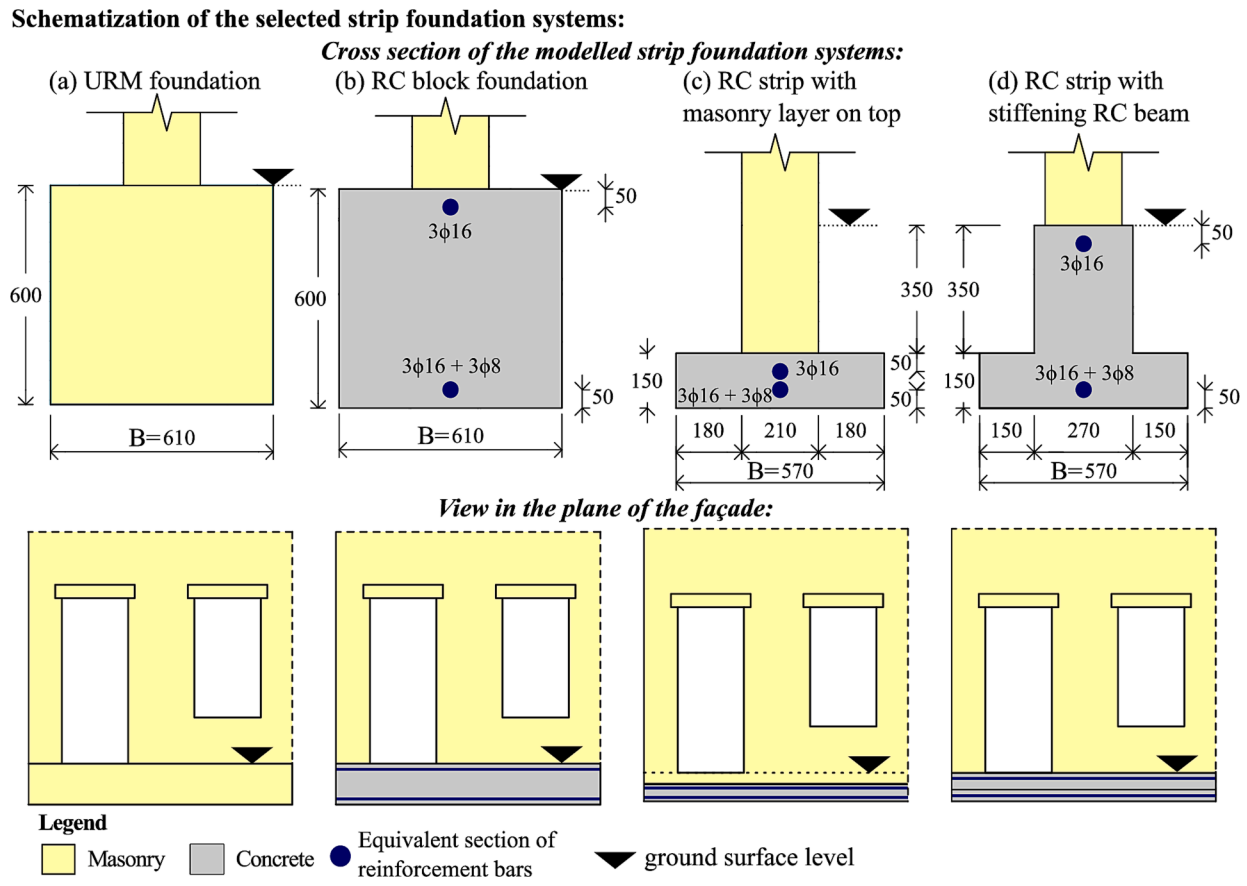

Fig. 4. Schematization of the recurrent strip foundation systems in the Netherlands: (a) URM foundation, (b) RC block foundation, (c) RC strip with masonry layer on top and (d) RC strip with stiffening RC beam. The level of the ground surface and the view in the plane of the façade is shown for each foundation system. Upper and lower reinforcement bars are represented as equivalent embedded bars. The equivalent section of each bar was based on design values of existing structures. Measures in millimeters.

Table 1
Adopter material properties for the masonry in the numerical models.

Material Properties	Symbol	Unit of measure	M1	M2	M3	M4	M5
Young's modulus vertical direction	E_y	[MPa]	2500	5000	6000	4000	7500
Young's modulus horizontal direction	E_x	[MPa]	1250	2500	3000	2000	3750
Shear Modulus	G_{xy}	[MPa]	1000	2000	2500	1650	3000
Bed joint tensile strength	f_{ty}	[MPa]	0.050	0.100	0.200	0.100	0.200
Fracture energy in tension	$G_{t,I}$	[N/mm]	0.003	0.010	0.010	0.010	0.020
Compressive strength	f_c	[MPa]	4.25	8.50	10.00	7.00	10.00
Fracture energy in compression	G_c	[N/mm]	10.00	20.00	15.00	15.00	20.00
Friction angle	φ	[rad]	0.500	0.700	0.900	0.400	0.600
Cohesion	c	[MPa]	0.075	0.150	0.300	0.150	0.200
Fracture energy in shear	G_s	[N/mm]	0.025	0.100	0.200	0.100	0.200
Mass Density	ρ	[Kg/m^3]	1708	1708	1708	1763	1763

Table 2
Adopted material properties for the reinforced concrete in the numerical models.

Material Properties	Symbol	Unit of measure	Concrete	Steel
Young's modulus	E	[MPa]	32,000	210,000
Poisson's ratio	ν	[-]	0.2	–
Fracture energy in tension	$G_{t,I}$	[N/mm]	0.137	–
Compressive strength	f_c	[MPa]	33	–
Mass density	ρ	[Kg/m^3]	2350	–
Yield strength	f_y	[MPa]	–	400
Hardening curve	–	–	–	No Hardening

$$K_n = \frac{GL}{1-\upsilon}\left[0.73 + 1.54\left(\frac{B}{L}\right)^{0.75}\right] \quad (2)$$

$$K_t = GL\left[\frac{1}{2-\upsilon}\left[2 + 2.5\left(\frac{B}{L}\right)^{0.85}\right] - \frac{0.2}{2(0.75-\upsilon)}\left[1 - \frac{B}{L}\right]\right] \quad (3)$$

Where K_n, and K_t from equations (2) and (3) represent the static stiffnesses for a rigid foundation respectively for the normal, and tangential (i.e. in the plane of the façade) directions to the soil surface. B represents the foundation thickness, while L is the foundation length (equal to the length of the façade) (Fig. 2). The properties of two soil types (Soil A and B in Table 4) were based on the superficial (i.e. the first five meters) soil stratigraphy in the Groningen region reported by

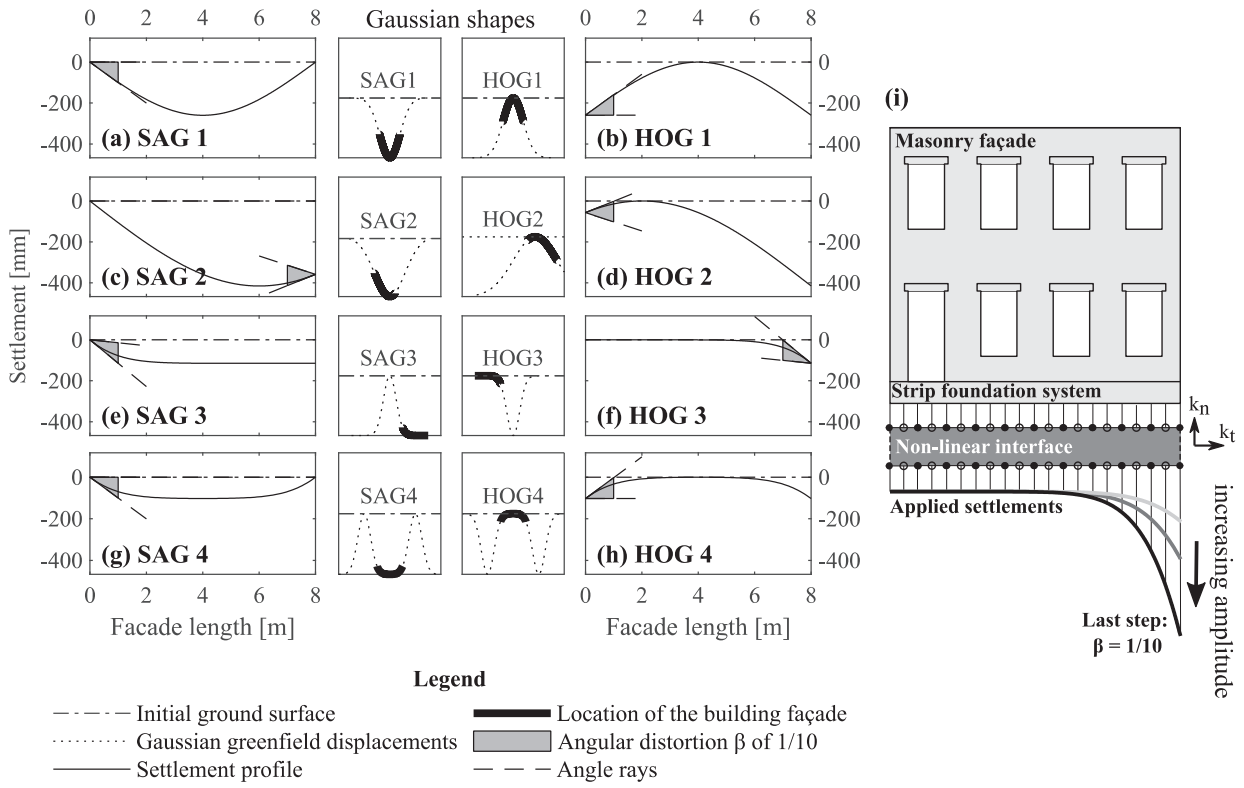

Fig. 5. The applied settlement profiles, that reproduce a loss of support underneath the strip foundation, computed from a Gaussian shape for a façade of 8 m and an angular distortion β equal to 1/10 (illustrated as a shaded area), defined according to the definition proposed by Burland and Wroth [2]: a) SAG1, b) HOG1, c) SAG2, d) HOG2, e) SAG3, f) HOG3, g) SAG4 and h) HOG4. All profiles were obtained by considering different positions of the façade over the displacement distributions, as schematically indicated in the centre pictures. The settlement shapes are applied in the numerical model with increasing amplitude as illustrated in i).

Table 3
Characteristics of the iterative scheme.

Load	Method	Convergence norm	Convergence tolerance	Satisfy all specified norms	Max. number of iterations
Gravity	Quasi-Newton	Displacement	0.01	Yes	200
		Force	0.01		
		Energy	0.001		
Settlement	Quasi-Newton	Energy	0.0001	Yes	200

Table 4
Material properties of the soil types considered.

Material Properties	Symbol	Unit of measure	Soil A	Soil B
Soil Material	[-]	[-]	Sandy soil	Clayey Soil
Shear Modulus	G	[MPa]	35	10
Poisson's Ratio	υ	[-]	0.3	0.45

Deltares [28]. In particular, G represents the small-strain shear modulus:

The use of equations (2) and (3) has been validated in previous studies [27,29–33]. The values of K_n, and K_t were then divided by B and L to obtain smeared values of the normal and shear linear stiffness (namely k_n, and k_t respectively, in Fig. 2 and Fig. 5) along the foundation footprint. For the purpose of the sensitivity analysis, a simulation is performed considering a Mohr-Coulomb interface to investigate the role of the soil-foundation contact friction. The analyses were performed by considering the same stiffness values (i.e. k_n , and k_t), and an arbitrarily-defined friction angle of 30° and zero cohesion for soil A in Table 4.

2.5. Method to characterize and quantify the damage

The severity of damage to buildings induced by ground displacements is measured with the damage classification proposed by Burland et al. [34] which is based on the ease of repair and the approximate width of the visible cracking. However, the objective quantification of the cracking damage requires considering not only the width, but also the length and the number of cracks in brick walls [7,8]. In this study, a parameter Ψ in equation (5) proposed by Korswagen et al. [7] was employed to quantify the resulting progression and accumulation of the damage in the numerical models in one single scalar value:

$$\Psi = 2{n_c}^{0.15}{\widehat{c}_w}^{0.3} \tag{4}$$

Where n_c is the number of cracks, $\widehat{c}_w$ is the width-weighted and length averaged crack width (in mm) calculated with equation (6):

$$\widehat{c}_w = \frac{\sum_{i=1}^{n_c} {c_{w,i}}^2 c_{L,i}}{\sum_{i=1}^{n_c} c_{w,i} c_{L,i}} \tag{5}$$

Where $c_{w,i}$ is the maximum crack width along the i-crack in mm, while $c_{L,i}$ is the i-crack length in mm. The parameter Ψ was computed considering the output of the FE analyses, not including the foundation and the lateral beam elements. The length of each crack is computed according to its shape (automatically classified by the script as horizontal, vertical or staircase-like).

A summary of the relation between Ψ and the approximate crack

width for the various damage levels proposed by Korswagen et al. [7], is presented in Table 5. It is worth stressing that Ψ is limited to the assessment of the light damage (i.e. up to crack of about 5 mm wide), whereas damage that could affect the structural safety would require a different metric, possibly quantifying the reduction of the capacity of the structure.

3. Results of the FE models

3.1. Relationship between settlement troughs and damage

Fig. 6 shows how the crack pattern (i.e. cracks' orientation, width, length, number) varies depending on the considered shape of the settlements and the applied distortion. The models depict how cracks initiate around the corners of the openings, and in most cases propagate mainly either horizontally or vertically (Fig. 6). Less frequently, some cracks develop diagonally (e.g. crack "2″ in Fig. 6h).

Thanks to the presence of lateral beam elements, cracking never initiates from the façade's edges [9]. The observed crack patterns were validated against available literature data (e.g.[35–37]). As discussed in section 2.3, each settlement profile was applied with a progressively increasing angular distortion in the FE model, allowing to record the vertical displacements of all the models at the façade's base (top edge of the foundation) for each step of the analysis. Accordingly, the four SRIs considered were computed both for the applied and the retrieved settlements (e.g., $\beta_{applied}$ refers to the applied angular distortion, while $\beta_{retrieved}$ corresponds to the one computed from the resulting displacements of the façade). In the following sections, the differences between the values of both the applied and retrieved parameters for each Ψ values are presented per FE model variation (discussed in section 2). The model of the façade with L/H = 1.14 (Fig. 3f), M2 (Table 1) with DW thickness (i.e. 210 mm) and an opening percentage = 0.27 (Fig. 3f), resting on the soil A (Table 4) on an URM foundation (Fig. 4a) is arbitrary assumed to be the reference case.

3.2. Influence of the settlement configurations

For the reference case, the influence of each settlement shape on the applied against retrieved SRI is shown in Fig. 7. A dashed line represents an idealization for which the applied and the retrieved parameters would be equal. The differences between applied and retrieved SRIs strongly depend on the shape of settlement (Fig. 7). Due to this dependency, in the following sections, the results will be mainly presented referring to the angular distortion, chosen for consistency with previous studies [20–23]. Moreover, the average values among the results of the eight settlement profiles is considered for both the applied and retrieved angular distortion, allowing to remove the dependency of the results from the settlement configurations. To keep a consistent comparison with other analyses, for those models, in which less than eight profiles reach a given Ψ value, the average value is omitted from the charts. The hogging and sagging settlement profiles exhibit the attainment of a given Ψ value for the same value of angular distortion, with the exception of the profiles HOG3 (Fig. 5f) and HOG4 (Fig. 5h). For these two profiles the distortion is localized in one side of the façade, contrary to the other settlement shapes.

Table 5
Damage scale with classification of visible damage based on the crack width and discretization of the damage parameter in sub-levels (adapted from Burland et al. [34], and Korswagen et al. [7]).

Damage level	Degree of damage	Approximate crack width	Parameter of damage
DL0	No Damage	Imperceptible cracks	$\Psi < 1$
DL1	Negligible	up to 0.1 mm	$1 \leq \Psi < 1.5$
DL2	Very slight	up to 1 mm	$1.5 \leq \Psi < 2.5$
DL3	Slight	up to 5 mm	$2.5 \leq \Psi < 3.5$
DL4	Moderate	5 to 15 mm	$\Psi \geq 3.5$

3.3. Influence of the material properties

In Fig. 8a, the applied angular distortion is plotted against the retrieved one for each masonry typology. The results show that the ratio between the applied and the measured angular distortion ranges from about 2 up to 51. Moreover, the façade model with M5 does not reach a damage higher than $\Psi = 1.0$. The lowest differences between applied and retrieved SRIs are observed for M1, which represent a very weak material. The results of the material M2 were compared with a model in which the elastic parameters (i.e. E_x, E_y and G_{xy} in Table 1) were further reduced by an order of magnitude, to investigate the role of the façade stiffness. The comparison proposed in Fig. 8b shows indeed that the model with reduced elastic properties (and therefore associated with a more flexible behaviour) reaches all the damage levels for values of the applied distortions smaller than the other materials, and it also exhibits the smallest differences between the applied and retrieved distortions; while an order of magnitude of difference between the elastic parameters represents an extreme condition, it serves to highlight this observation.

3.4. Effects of the façade features

The results for the models with different L/H ratios (Fig. 3) are presented in Fig. 9 using a log–log plot, to better illustrate the distinctions. Façades with a L/H lower or equal than 1.00 were observed to not reach a Ψ value higher than 1.50 in any of the models, while only for few settlement profiles a Ψ value of 1.00 is reached. A decrease in the L/H ratio (i.e. squat facades) is associated with less damage, and with a bigger difference between applied and retrieved parameters.

The effects of the additional variations of the façade features are shown in Fig. 10. A simulation is performed doubling the mass of the reference façade's masonry material (M2). Fig. 10a shows how an increase in the mass density leads to damage for smaller values of the applied angular distortion, compared to the reference case. This effect could occur particularly when the loads of the storeys and/or the roof of the building is summed to the self-weight of the façade.

The influence of the opening percentage was investigated comparing the results for the models in Fig. 3g and Fig. 3h (which correspond to an opening percentage of 10% and 20% respectively) with the reference case. The results of these analyses are proposed in Fig. 10b. The façade with the smallest opening percentage (i.e. 10%) does not exhibit cracks wider than 0.1 mm (Ψ value higher than 1.0). As observed in the case of the elastic parameters, façades with large openings have a more flexible response and more damage, in agreement with the findings of previous studies (i.e. [36,38]). Fig. 10c shows the comparison between the reference FE model and one without the inclusion of the lateral beam elements (Fig. 2). For the model without lateral beam elements, the damage initially progresses similarly to the reference case and suddenly increases after reaching a value of Ψ equal to 1.5; the removal of the lateral beam elements decreases the difference between the applied and the retrieved angular distortion.

3.5. Influence of the foundation, soil and interface

Fig. 11 shows how the façades on RC foundations exhibit a stiffer behaviour and consequently, on average, less damage. The influence of the interface features is shown in Fig. 12. To investigate the role of the soil stiffness relatively to the façade, a sensitivity analysis was performed by varying the adopted interface stiffness. Two variations were selected by increasing and decreasing the values of normal and tangential stiffness of the reference model by an order of magnitude (k_n, k_t)*10, and (k_n, k_t)*/10 in Fig. 12a. The smallest difference between the applied and the retrieved angular distortion are observed in the case of the highest stiffnesses values, (k_n, k_t)*10. Similarly, Fig. 12b shows the

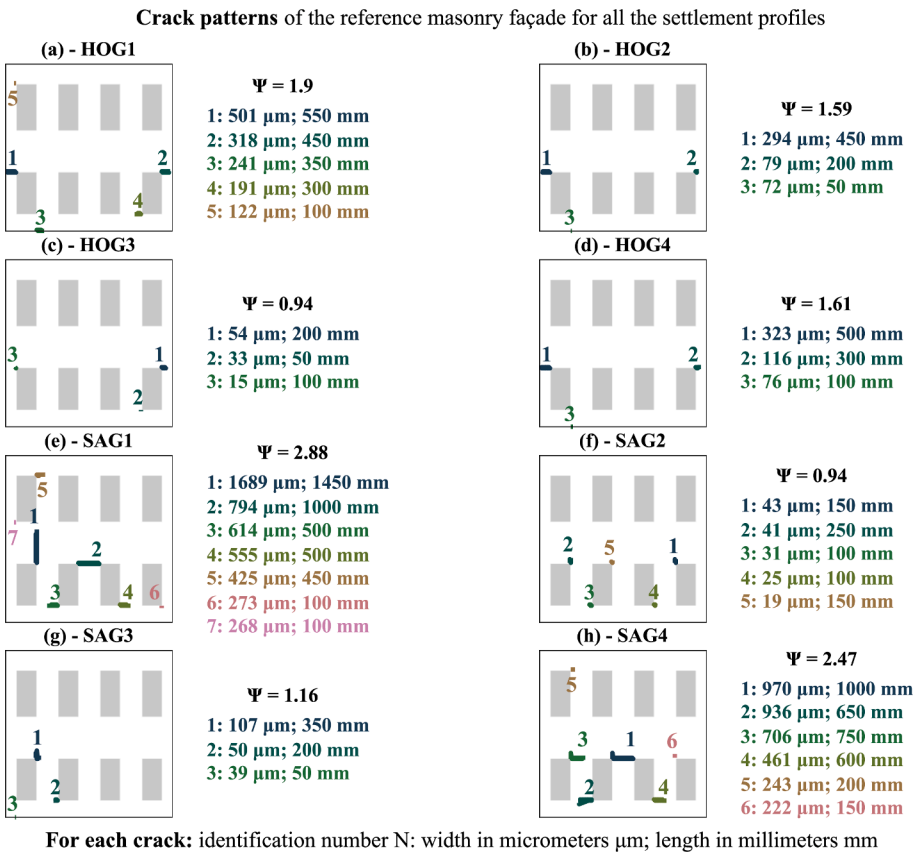

Fig. 6. Crack patterns of the masonry façade for all the settlement profiles at step 60 (maximum applied settlement equals to about 11 mm) of the numerical model: a) HOG1, b) HOG2, c) HOG3, d) HOG,4 e) SAG1, f) SAG2, g) SAG3 and h) SAG4. Note that for a given numerical step the applied settlement configurations are not characterized by the same value of the angular distortion, due to the variable load step, as discussed in section 2. The cracks' width in the plots is exaggerated.

comparison between the reference model resting on sand (Soil A in Table 4) and a variation resting on clay (Soil B in Table 4), thus contrasting the shear modulus and the Poisson's ratio.

Interestingly, the model resting on a clayey soil exhibits less damage compared to the one on sand. The façade acts stiffer on the clayey soil than on the sandy one, thus increasing the differences between applied and retrieved displacements and leading to less damage. Fig. 12c shows the comparison between the use of a smooth or a rough interface for the reference model, as described in section 2.4. Interestingly, the two analyses show similar results when Ψ is smaller than 1.5. However, the model with a rough interface is more susceptible to damage, as the damage occurs for smaller values of the angular distortion when compared with the reference case [39].

3.6. Results of the sensitivity analyses

In Fig. 13 an overview of the results of all the models is presented. Particularly, the mean applied angular distortion of each model is divided by the one of the reference case so that the effect of all the investigated variations can be compared. The L/H ratio is the one that is associated with the larger variability of the structural response. Accordingly, for the values of Ψ equal to 0.5 and 3.5, the mean applied angular distortion β_a ranges from values 4 times smaller (in the case of slender façade with high L/H values) to 9 times higher (for squat façades with small L/H values) compared to the reference case (L/H = 1.14). A similar effect is observed when comparing the analyses with stiffer or softer interfaces. In the case of the foundation system, the RC strip foundation reaches a Ψ of 0.5 for values of β_a about 2 times higher than the reference case, thus with a stiffer response. In comparison, higher Ψ values are not possible, as RC strip foundations don't exceed Ψ equal to 0.5. A similar effect is given by the opening percentage: models with a small opening percentage present values of β_a about 4 times higher than the reference case. Other parameters have a smaller influence on the results.

3.7. Differences between applied and retrieved settlements

Many authors investigated the relationship between the ground displacements and the building deformation by means of the modification factor (MD); This factor corresponds to the ratio between the deflection ratio computed from deformation of the building and the one of the green field profile [40–44], for tunnelling and excavations. The deflection ratio and the MD values were computed for all analyses herein presented, allowing to compare the results with the state of the art. The MD factor is plotted against a dimensionless ratio, made up from the relative bending stiffness [40], that takes into account the role of the relative stiffness between the soil and the building. It should be noted that the relative bending stiffness ρ is typically computed per meter stretch in the direction perpendicular to the building length, since it was originally proposed with reference to plain-strain numerical analyses [40]. Based on field data and experimental tests, Goh and Mair (2011) [44] introduced the following expression (6):

$$\rho = \frac{EI}{E_s L^3 W} \tag{6}$$

where EI is the masonry façade stiffness, E_s a representative soil stiffness and L the length of the building in either hogging or sagging based on the greenfield settlement profile (equal to the length of the façade in this study) and W is the building width. In this study, the relative bending stiffness ρ is computed with (6), assuming W equal to L. In particular, in

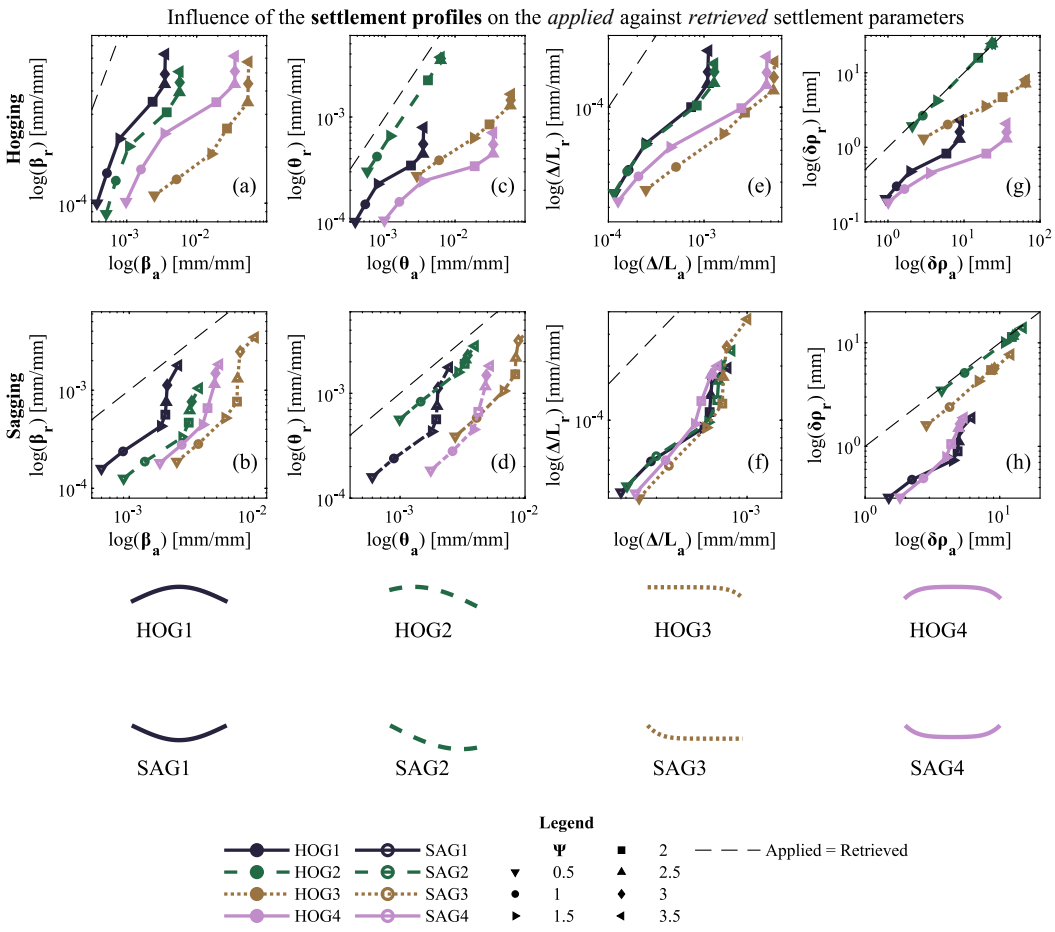

Fig. 7. Influence of the settlement configuration on the applied vs. retrieved settlement parameters for each level of damage for: angular distortion for a) hogging and b) sagging, rotation for c) hogging and d) sagging, deflection ratio for e) hogging and f) sagging, differential settlement for g) hogging and h) sagging. The shapes of the settlement profiles (not to scale) are shown for clarity. Plots in the logarithmic scale.

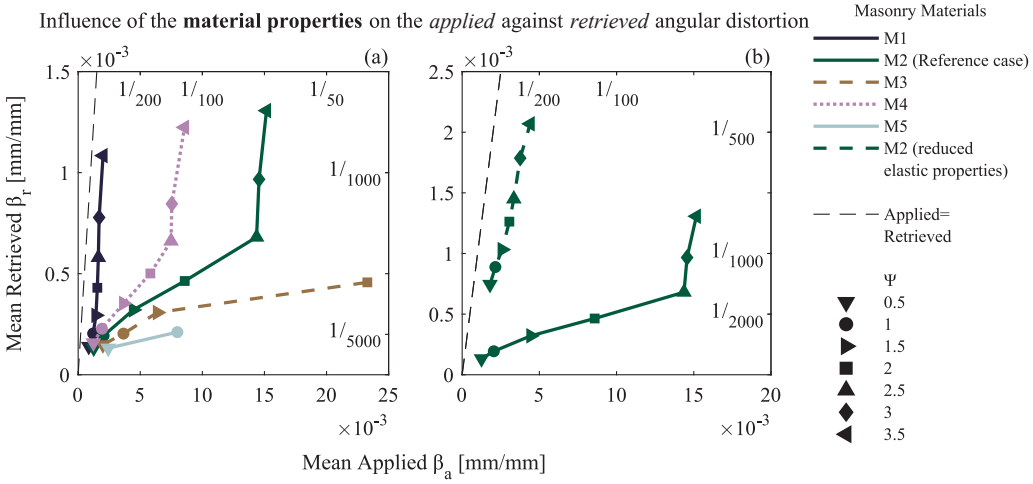

Fig. 8. Differences of the applied vs. retrieved angular distortion for each level of damage for the variation of the: a) material typology, b) variation of the elastic parameters. The secondary x- and y- axes (on top and on the right of the plots) show the values of the angular distortion as $1/\beta^{-1}$, as typically adopted in the literature.

this study EI is estimated with (7), similarly to [45]:

$$EI = E_w I_w \alpha_r + E_f I_f \tag{7}$$

Where E_w is the Young's modulus of the masonry, I_w is the second moment of inertia of the façade, while $E_f I_f$ is the contribution of the foundation.

In particular, I_w is computed by assuming the neutral axis close to the mid-height of the façade in sagging and equal to the top edge of the foundation in hogging [2]. The moment of inertia I_f of the foundation is computed relative to its own middle plane [45]. Moreover, α_r represents the reduction factor to consider the presence of voids (doors or windows), as proposed by Melis and Ortiz [45], reported in Table 6:

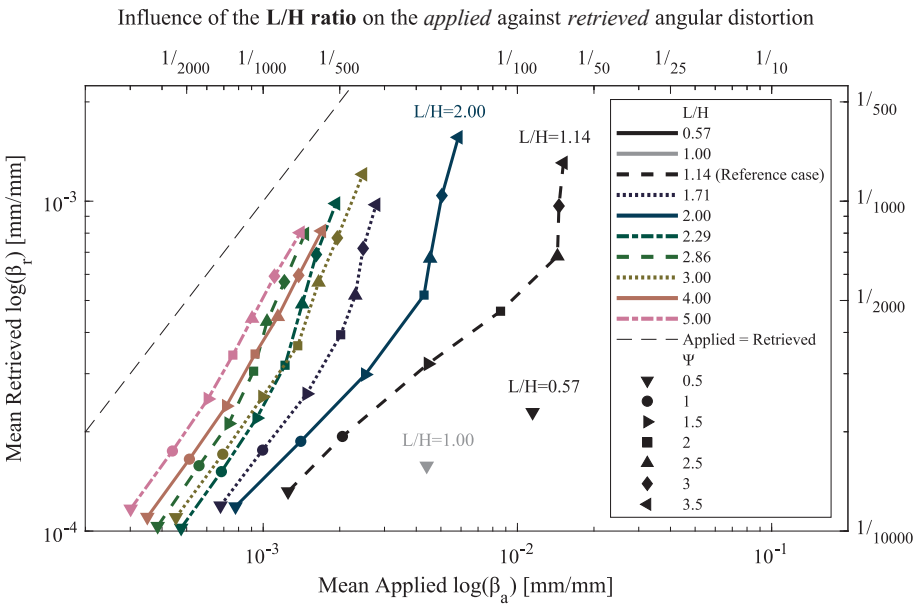

Fig. 9. Influence of the length over height (L/H) ratio on the difference between applied vs. retrieved angular distortion. The secondary x- and y- axes (on top and on the right of the plots) show the values of the angular distortion as $1/\beta^{-1}$, as typically adopted in the literature. Plot in the logarithmic scale.

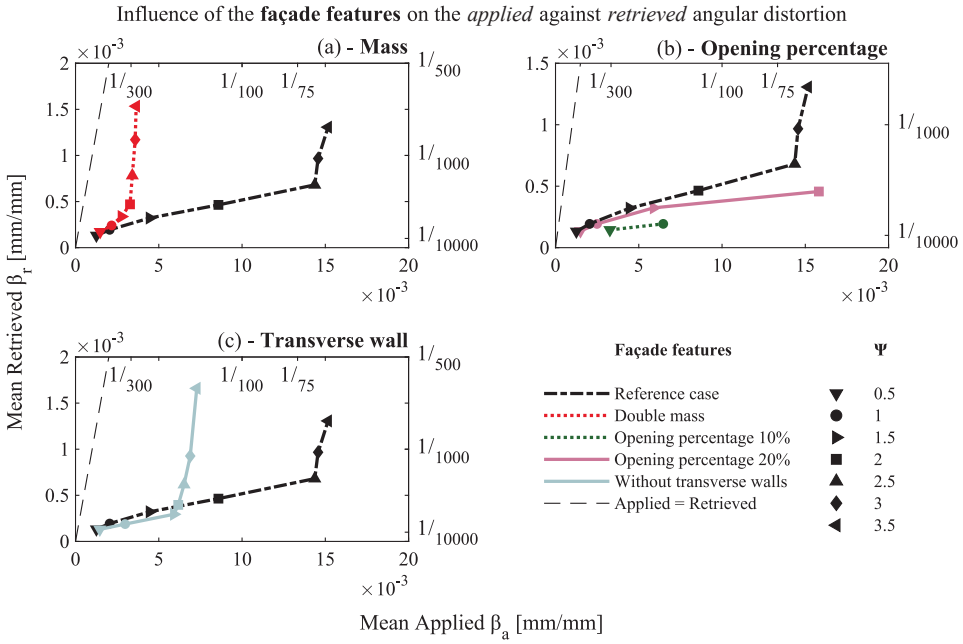

Fig. 10. Differences of the applied vs. retrieved angular distortion for each level of damage for the variation of the: a) mass density, b) opening percentage and c) presence of the transverse walls. The secondary x- and y- axes (on top and on the right of the plots) show the values of the angular distortion as $1/\beta^{-1}$, as typically adopted in the literature.

The modification factors are compared to the design curves proposed by Mair (2013) [41] in Fig. 14. The points found lay between the two design curves (Fig. 14). Interestingly, the values of the modification factor increase for higher level of damage (higher Ψ values). As cracking develops the stiffness of the building may decrease significantly, allowing the building to conform more closely to the assumed ground movement [38,46].

3.8. Comparison with the available limit values

In Fig. 15 the cumulative density functions (or exceedance curve) are retrieved for all the selected SRI parameters (i.e. angular distortion, rotation, deflection ratio and differential settlement) for Ψ values ranging from 0.5 to 3.5. The exceedance curves were obtained counting the number of models that exceed each threshold of damage (Ψ) in relation to the total number of analyses. It should be highlighted that the exceedance curves do not provide probabilistic information regarding the real population of masonry buildings, but only an insight on the results of the numerical analyses of this study. A more comprehensive analysis would require modelling a wider, realistic, set of cases and combinations of the investigated parameters.

The limit values of the settlement parameters, often employed as guidelines or recommendations (e.g. in [2,4,5,20,47–49]), are herein discussed in relation to the result of the numerical analyses proposed in

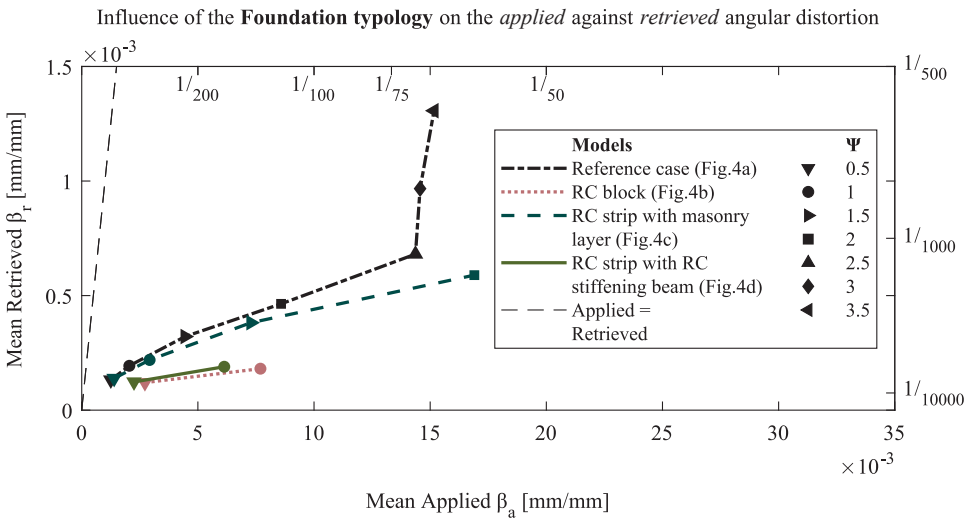

Fig. 11. Differences of the applied vs. retrieved angular distortion for each level of damage for the variation of the foundation typology. The secondary x- and y- axes (on top and on the right of the plots) show the values of the angular distortion as $1/\beta^{-1}$, as typically adopted in the literature.

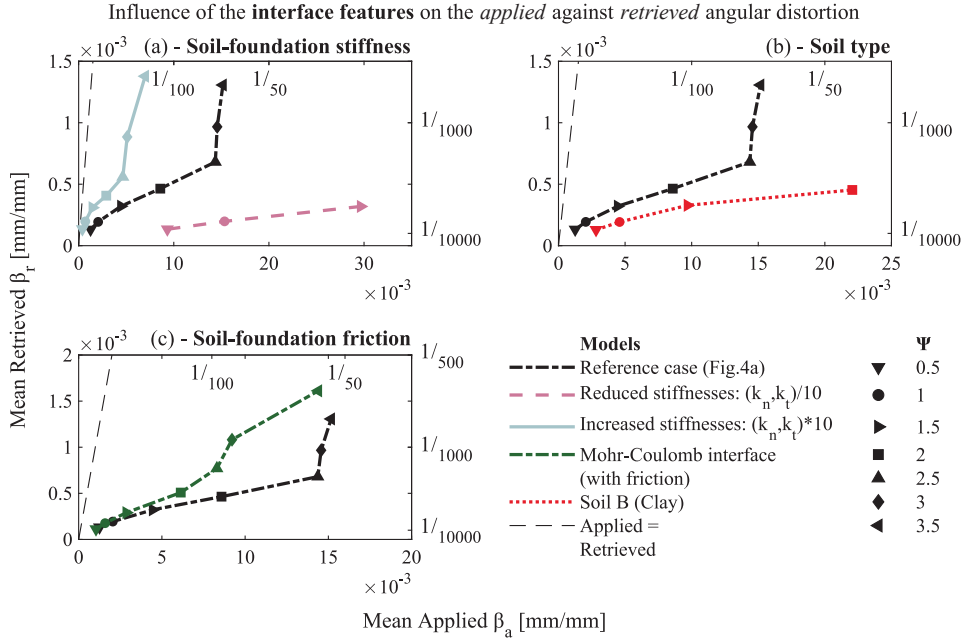

Fig. 12. Differences of the applied vs. retrieved angular distortion for each level of damage for the variation of the: a) interface stiffness, b) interface model, c) soil type. The secondary x- and y- axes (on top and on the right of the plots) show the values of the angular distortion as $1/\beta^{-1}$, as typically adopted in the literature.

this study. For each threshold, the probability of exceedance for the corresponding Ψ value is retrieved from the cumulative density functions shown in Fig. 15. This allows assessing the performance of such limit values relatively to the numerical analyses presented in this study. An overview of the available literature thresholds, in terms of the structures' angular distortion β and deflection ratio Δ/L, thus the "retrieved" settlement parameters, is presented in Table 7. Regarding other parameters, only a limited number of studies focus on the rotation and the differential settlements. For the rotation, there is a lack of limit values in the current state of art. In the case of the differential settlement, however, this parameter may not be sufficiently reliable in the definition of the relationship between the ground settlement and the resulting damage. For instance, although the differential settlement can be arguably easily computed in many cases, it does not provide any information regarding the distortion along the building. The differential settlements could also result from the uniform tilting of the building with small or null distortions in the structure unlikely to produce damage [12]. For each limit value in Table 7, the corresponding probability of exceedance is reported from the curves of the retrieved settlement parameters (Fig. 15). In all the encountered cases, if the goal is to prevent the occurrence of a Ψ value, the high probabilities of exceedance discussed indicate how the limit values may be too optimistic in relation to the results of the numerical model.

For example, a Ψ higher or equal to 3.5 is associated with the occurrence of cracks above 5 mm wide (in this study), corresponding to the occurrence of a serviceability limit state [47,50]. In the Eurocode [48], the threshold values of the angular distortion β corresponding to the occurrence of a serviceability limit state ranges from 1/4000 to 1/300 depending on the shape of the settlement profile (Table 7). For such values of angular distortion, from 10 to 75 % of the models reach or exceed a Ψ of 3.5, thus the thresholds proposed in the guideline are observed to be too optimistic with respect to the results of this study.

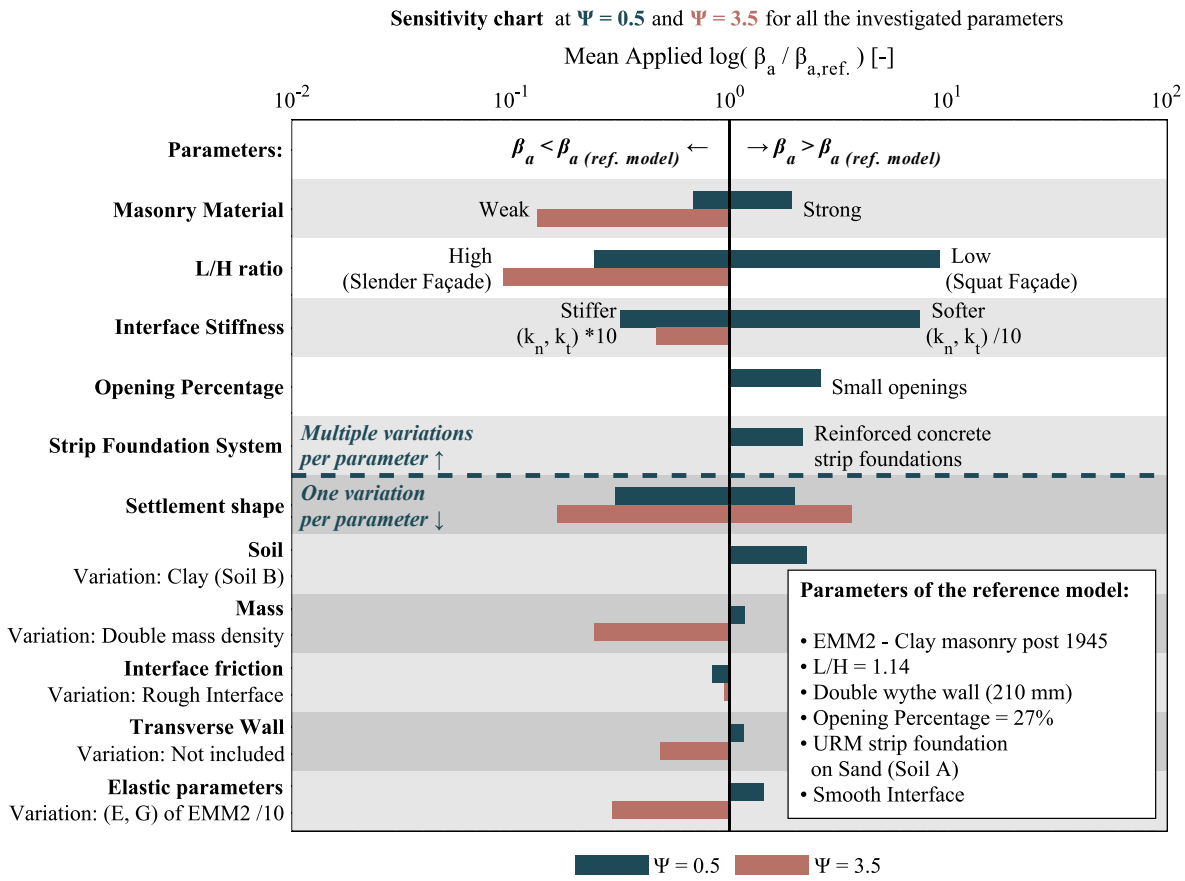

Fig. 13. Sensitivity chart of the results of all the numerical models. The x-axis in the logarithmic scale shows the ratio between the mean applied angular distortion β_a and the one of the reference model. The results are categorized by the number of models used to study the influence of each parameter by a dashed line.

Table 6
Reduction factor of wall bending stiffness EI (from Melis and Ortiz [45]).

Type of wall	L < 2H	L > 2H
Opening from 0 to 15%	0.70	0.90
Opening from 15 to 25%	0.40	0.60
Opening from 25 to 40%	0.10	0.15

4. Discussion

This study focuses on the settlements due to a combination of subsidence drivers (e.g. organic soil oxidation, groundwater lowering, soil shrinkage) in urban areas. Detailed measurements of the ground settlements along strip foundation footprints are not available in the state of the art. Thus, the shapes of the imposed settlements, conformed to a Gaussian curve, fictitiously simulate the loss of support underneath the foundations without having the soil unrealistically pull on the foundations. Urban subsidence phenomena are characterized by smaller horizontal components of the ground movements compared to excavations, tunnelling or mining works [4]; Thus the horizontal ground deformations were purposively neglected. A smooth interface was assumed for the analyses, due to the limited empirical knowledge of the transmission of the stresses and displacements from the soil to the foundations. However, a rough soil-foundation interface was observed to reduce the ratio between the applied and retrieved settlement deformations when compared to the smooth one. Further improvements may include the effects given by the soil embedding the RC strip foundations (Fig. 4c and d).

The geometry of the reference case is inspired by the ones of typical masonry structures. Further improvements of the 2D modelling approach of the structure may include the calibration of the thickness of the lateral beam elements against a 3D model to better represent the effects of the house-to-house separation walls.

5. Conclusions

The sensitivity analysis presented herein was carried out to investigate the non-linear response of the masonry façades subjected to different settlement shapes underneath their strip foundations. The effect of different buildings' features, material properties and settlement profiles was studied; Thus, we have observed:

- The results of the numerical analyses in terms of damage and deformation strongly vary depending on the shapes of the applied settlements.
- As the damage increases, the façade tends to be more flexible, thus better accommodating the imposed settlement deformations.
- The façades on reinforced concrete strip foundations were observed, on average, to exhibit lower levels of damage with respect to the masonry ones.
- The façades with L/H smaller or equal to 1 were observed to have cracks of maximum 1 mm, on average, without further progression of the damage afterwards, even for high values of the applied angular distortion (such as 0.1 or 1/10).
- On the contrary, some of the façades with L/H higher than 1 exhibit cracks equal to or wider than 5 mm for applied angular distortion of 0.35 ‰ (or 1/2833).
- The limit values of the settlement parameters (i.e. angular distortion, deflection ratio, differential settlement, rotation) proposed in (inter) national codes and guidelines were observed to be too optimistic compared to the results of the FE models herein presented.

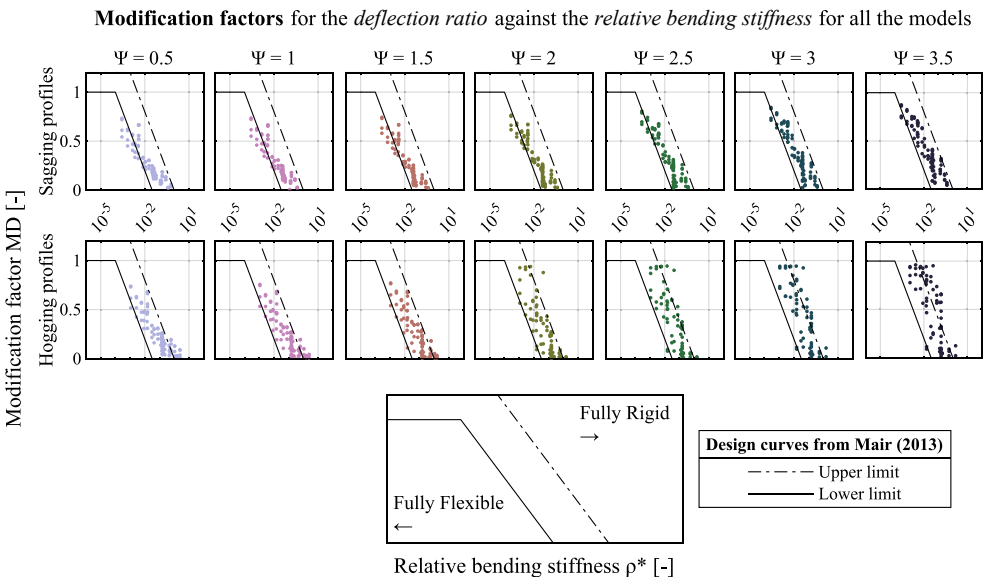

Fig. 14. Modification factors for the deflection ratio with relative bending stiffness for all Ψ values. Design curves from Mair, (2013) [41]. The results refer to all the façade models and all the settlement profiles.

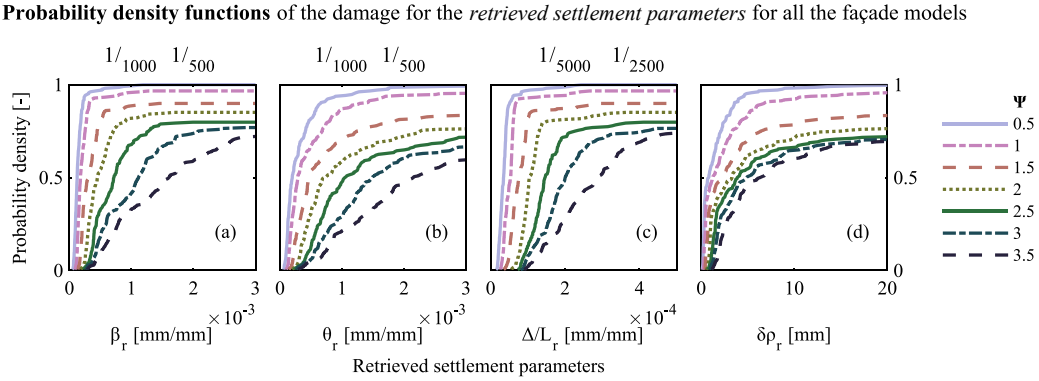

Fig. 15. Cumulative density function for all the Ψ values for the retrieved: (a) angular distortion β_r, (b) rotation θ_r, (c) deflection ratio Δ/L_r and (d) differential settlement $\delta\rho_r$. The secondary x- axes (on top of the plots of the (a) angular distortion, (b) rotation and (c) deflection ratio) show the values of the parameters as $1/x^{-1}$, as typically adopted in the literature.

Table 7
Overview of the available literature limit values [1,2,4,5,20,47–50] with the estimated Ψ values and corresponding probabilities of exceedance.

Reference	Parameter	Values [‰]	Ratio [1/ β^{-1}]	Description	This study	
					Ψ	Probability [%]
Meyerhof, 1982	β	0.5	1/2000	Safe limit for hogging	1.0	93
		1.0	1/1000	Safe limit for sagging	1.0	96
EN 1997–1 (2004)	β	0.5 to 3.3	1/2000 to 1/300	sagging (serviceability limit state)	3.5	10 to 75
		0.25 to 1.7	1/4000 to 1/600	hogging (serviceability limit state)	3.5	0 to 52
Boscardin and	β	1.5	1/667	Very slight damage (self weight)	2.5	79
Cording, 1989		3.3	1/300	Slight damage (self weight)	3.5	75
Zhang and Ng., 2007	β	0.9	1/1100	Tolerable limit (load bearing walls)	1.0	96
		1.2	1/800	Tolerable limit (shallow foundations)	1.0	97
Polshin and Tokar, 1957	Δ/L	0.3 to 0.4	1/3300 to 1/2500	with L/H ≤ 3	1.5	89
		0.5 to 0.7	1/2000 to 1/1400	with L/H ≥ 5	1.5	89
		0.5	1/2000	no cracking limit	1.0	97
Burland et al. 1975	Δ/L	0.2 ‰	1/5000	Limit value for L/H = 1	1.5	88

The results of this study are therefore propaedeutic for the development of probabilistic frameworks and damage assessment tools for masonry structures subjected to settlement.

CRediT authorship contribution statement

Alfonso Prosperi: Conceptualization, Methodology, Software, Formal analysis, Investigation, Data curation, Writing – review & editing. **Michele Longo:** Conceptualization, Methodology, Software, Formal analysis, Investigation, Data curation, Writing – review &

editing. **Paul A. Korswagen:** Conceptualization, Methodology, Software, Supervision, Writing – review & editing. **Mandy Korff:** Conceptualization, Supervision, Funding acquisition. **Jan G. Rots:** Conceptualization, Supervision, Funding acquisition.

Declaration of Competing Interest

The authors declare that they have no known competing financial interests or personal relationships that could have appeared to influence the work reported in this paper.

Data availability

No data was used for the research described in the article.

Acknowledgments

The research presented in this paper is part of the project Living on Soft Soils: Subsidence and Society (grantnr.: NWA.1160.18.259). This project is funded through the Dutch Research Council (NWO-NWA-ORC), Utrecht University, Wageningen University, Delft University of Technology, Ministry of Infrastructure & Water Management, Ministry of the Interior & Kingdom Relations, Deltares, Wageningen Environmental Research, TNO-Geological Survey of The Netherlands, STOWA, Water Authority: Hoogheemraadschap de Stichtse Rijnlanden, Water Authority: Drents Overijsselse Delta, Province of Utrecht, Province of Zuid-Holland, Municipality of Gouda, Platform Soft Soil, Sweco, Tauw BV, NAM.

References

[1] Skempton AW, MacDonald DH. The allowable settlements of buildings. Proceedings of the Institution of Civil Engineers. 1956;5:727-68.
[2] Burland JB, Wroth C. Settlement of buildings and associated damage. 1975.
[3] Bjerrum L. Allowable settlement of structures. Proceedings of the 3rd European Conference on Soil Mechanics and Foundation Engineering, Wiesbaden, Germany1963. p. 135-7.
[4] Boscardin MD, Cording EJ. Building response to excavation-induced settlement. J Geotech Eng-Asce 1989;115:1–21.
[5] Polshin DE, Tokar R. Maximum allowable non-uniform settlement of structures. Proc, 4th Int Conf on Soil Mechanics and Foundation Engineering: Butterworth's London; 1957. p. 402-5.
[6] Peduto D, Korff M, Nicodemo G, Marchese A, Ferlisi S. Empirical fragility curves for settlement-affected buildings: analysis of different intensity parameters for seven hundred masonry buildings in The Netherlands. Soils Found 2019;59:380–97.
[7] Korswagen PA, Longo M, Meulman E, Rots JG. Crack initiation and propagation in unreinforced masonry specimens subjected to repeated in-plane loading during light damage. Bull Earthq Eng 2019;17:4651–87.
[8] Korswagen PA, Jonkman SN, Terwel KC. Probabilistic assessment of structural damage from coupled multi-hazards. Struct Saf 2019;76:135–48.
[9] Korswagen PA, Longo M, Meulman E, Rots J. Experimental and computational study of the influence of pre-damage patterns in unreinforced masonry crack propagation due to induced, repeated earthquakes. 13th North American Masonry Conference: TMS; 2019. p. 1628-45.
[10] DIANA FEA. Finite Element Analysis User's Manual - Release 10.5. Delft, The Netherlands: DIANA FEA BV, 2021.2021.
[11] Rots JG, Korswagen PA, Longo M. Computational modelling checks of masonry building damage due to deep subsidence. Delft University of Technology; 2021.
[12] Charles JA, Skinner HD. Settlement and tilt of low-rise buildings. Proceedings of the Institution of Civil Engineers-Geotechnical Engineering. 2004;157:65-75.
[13] Van Staalduinen P, Rots J, Terwel K. Onderzoek naar de oorzaken van bouwkundige schade in Groningen: Methodologie en case studies ter duiding vande oorzaken. 2019.
[14] Giardina G, Van de Graaf AV, Hendriks MAN, Rots JG, Marini A. Numerical analysis of a masonry facade subject to tunnelling-induced settlements. Eng Struct 2013;54:234–47.
[15] NPR9998:2020en. Assessment of structural safety of buildings in case of erection, reconstruction and disapproval - Induced earthquakes - Basis of design, actions and resistances. 2021.
[16] Schreppers G, Garofano A, Messali F, Rots J. DIANA validation report for masonry modelling. DIANA FEA Report 2016.
[17] Korswagen Eguren PA, Longo M, Meulman E, van Hoogdalem C. Damage sensitivity of Groningen masonry structures–Experimental and computational studies: Stream 1. 2017.
[18] Rots J, Messali F, Esposito R, Jafari S, Mariani V. Computational Modelling of Masonry with a view to Groningen induced Seismicity. 10th SAHC Structural Analysis of Historical Construction. Leuven; 2016.
[19] Peck RB. Deep excavations and tunneling in soft ground. Proc 7th ICSMFE, 1969. 1969:225-90.
[20] Meyerhof GG. Limit states design in geotechnical engineering. Struct Saf 1982;1:67–71.
[21] Son M, Cording EJ. Estimation of building damage due to excavation-induced ground movements. J Geotech Geoenviron Eng 2005;131:162–77.
[22] Zhang LM, Ng AMY. Probabilistic limiting tolerable displacements for serviceability limit state design of foundations. Geotechnique 2005;55:151–61.
[23] Ang T, Masri K. Behaviour of residential structures on problematic ground. In: IOP Conference Series: Materials Science and Engineering. IOP Publishing; 2019. p. 012010.
[24] NEHRP. NIST GCR 12-917-21 Soil–structure interaction for building structures. Gaithersburg: National Institute of Standards and Technology, US Department of Commerce; 2012.
[25] Gazetas G. Foundation vibrations. Foundation engineering handbook: Springer; 1991. p. 553–93.
[26] Mylonakis G, Nikolaou S, Gazetas G. Footings under seismic loading: Analysis and design issues with emphasis on bridge foundations. Soil Dyn Earthq Eng 2006;26:824–53.
[27] Ferlisi S, Nicodemo G, Peduto D, Negulescu C, Grandjean G. Deterministic and probabilistic analyses of the 3D response of masonry buildings to imposed settlement troughs. Georisk-Assess Manage Risk Eng Syst Geohazards 2020;14:260–79.
[28] Kruiver P, de Lange G, Wiersma A, Meijers P, Korff M, Peeters J, et al. Geological schematisation of the shallow subsurface of Groningen—for site response to earthquakes for the Groningen gas field. Deltares Report 2015.
[29] Ferlisi S, Nicodemo G, Peduto D. Numerical analysis of the behaviour of masonry buildings undergoing differential settlements. 2019.
[30] Longo M, Sousamli M, Korswagen PA, van Staalduinen P, Rots JG. Sub-structure-based 'three-tiered' finite element approach to soil-masonry-wall interaction for light seismic motion. Eng Struct 2021;245:112847.
[31] Drougkas A, Verstrynge E, Szeker P, Heirman G, Bejarano-Urrego LE, Giardina G, et al. Numerical modeling of a Church Nave Wall subjected to differential settlements: soil-structure interaction, time-dependence and sensitivity analysis. Int J Arch Herit 2020;14:1221–38.
[32] Anastasopoulos I, Gerolymos N, Gazetas G, Bransby MF. Simplified approach for design of raft foundations against fault rupture. part II: soil-structure interaction. Earthq Eng Eng Vib 2008;7:165–79.
[33] Korswagen PA, Longo M, Rots JG. High-resolution monitoring of the initial development of cracks in experimental masonry shear walls and their reproduction in finite element models. Eng Struct 2020;211:110365.
[34] Burland JB, Broms BB, De Mello VF. Behaviour of foundations and structures. 1978.
[35] De Vent IAE. Prototype of a diagnostic decision support tool for structural damage in masonry. 2011.
[36] Giardina G, Rots J, Hendriks M. Modelling of settlement induced building damage. Delft: TU Delft; 2013.
[37] Peduto D, Nicodemo G, Maccabiani J, Ferlisi S. Multi-scale analysis of settlement-induced building damage using damage surveys and DInSAR data: a case study in The Netherlands. Eng Geol 2017;218:117–33.
[38] Son M, Cording EJ. Evaluation of building stiffness for building response analysis to excavation-induced ground movements. J Geotech Geoenviron Eng 2007;133:995–1002.
[39] Burd H, Yiu W, Acikgoz S, Martin C. Soil-foundation interaction model for the assessment of tunnelling-induced damage to masonry buildings. Tunn Undergr Space Technol 2022;119:104208.
[40] Potts DM, Addenbrooke TI. A structure's influence on tunnelling-induced ground movements. Proceedings of the Institution of Civil Engineers-Geotechnical Engineering. 1997;125:109-25.
[41] Mair R. Tunnelling and deep excavations: Ground movements and their effects. Proceedings of the 15th European Conference on Soil Mechanics and Geotechnical Engineering–Geotechnics of Hard Soils–Weak Rocks (Part 4) IOS Press, Amsterdam, the Netherlands2013. p. 39-70.
[42] Goh K. Response of ground and buildings to deep excavations and tunnelling. University of Cambridge; 2011.
[43] Franza A, Ritter S, Dejong MJ. Continuum solutions for tunnel–building interaction and a modified framework for deformation prediction. Géotechnique 2020;70:108–22.
[44] Goh K, Mair R. Building damage assessment for deep excavations in Singapore and the influence of building stiffness. Geotech Eng J SEAGS & AGSSEA 2011;42:1–12.
[45] Melis M, Rodriguez Ortiz J. Consideration of the stiffness of buildings in the estimation of subsidence damage by EPB tunnelling in the Madrid subway. International conference on the response of buildings to excavation induced ground movements2001. p. 387-94.
[46] Simpson BG, W.J.;. Discussion: The effect of groundmovements on rigid masonry facades. Proc, Int Symp on Geotech-nical Aspects of Underground Construction in Soft Ground. 1996:769–70.
[47] Rankin W. Ground movements resulting from urban tunnelling: predictions and effects. Geological Society, London, Engineering Geology Special Publications. 1988;5:79-92.

[48] CEN. Eurocode 7 Geotechnical design - Part 1: General rules. Final Draft, EN 1997-1:2004 (E), (F) and (G). European Committee for Standardization: Brussels2004. p. 168 pages (E).
[49] Zhang L, Ng AM. Limiting tolerable settlement and angular distortion for building foundations. Probabilist Appl Geotech Eng 2007:1–11.
[50] Yunusa GH, Hamza U, Abdulfatah AY, Suleiman A. Geotechnical investigation into the causes of cracks in building: a case study. Electron J Geotech Eng 2013;18:2823–33.